Maejo Int. J. Sci. Technol. **2010**, *4*(01), 159-168

Maejo International Journal of Science and Technology

ISSN 1905-7873
Available online at www.mijst.mju.ac.th

Full Paper

Semiclassical three-valley Monte Carlo simulation analysis of steady-state and transient electron transport within bulk $InAs_xP_{1-x}$, InAs and InP

Hadi Arabshahi* , Mahmoud R. Rokn-Abadi and Fatemeh Badieyan

Physics Department, Ferdowsi University of Mashhad, Mashhad, Iran

* Corresponding author, e-mail: arabshahi@um.ac.ir

Received: 2 December 2009 / Accepted: 20 April 2010 / Published: 20 April 2010

Abstract: We have studied how electrons, initially in thermal equilibrium, drift under the action of an applied electric field within bulk zincblende $InAs_xP_{1-x}$, InAs and InP. Calculations are made using a non-parabolic effective-mass energy band model. Monte Carlo simulation includes all of the major scattering mechanisms. The band parameters used in the simulation are extracted from optimised pseudo-potential band calculations to ensure excellent agreement with experimental information and ab-initio band models. The effects of alloy scattering on the electron transport physics are examined. For all materials, it is found that electron velocity overshoot only occurs when the electric field is increased to a value above a certain critical field, unique to each material. This critical field is strongly dependent on the material parameters. Transient velocity overshoot has also been simulated, with the sudden application of fields up to 1600 kVm^{-1}, appropriate to the gate-drain fields expected within an operational field-effect transistor. The electron drift velocity relaxes to the saturation value of about 1.5×10^5 ms^{-1} within 4 pico-seconds for all crystal structures. The steady-state and transient velocity overshoot characteristics are in fair agreement with other recent calculations.

Keywords: Monte Carlo simulation, steady-state electron transport, transient electron transport, pseudo-potential, alloy scattering, velocity overshoot, critical field

Maejo Int. J. Sci. Technol. **2010**, *4*(01), 159-168

Introduction

InP and InAs offer the prospect of mobility comparable to GaAs and are increasingly being developed for the construction of optical switches and optoelectronic devices. While GaAs has been extensively studied [1-3], InAs and InP and alloys constructed from them such as $InAs_xP_{1-x}$ have yet to be examined to the same extent. Alloys of InAs and InP have unfortunately proved to be difficult material to work with in practice and very little experimental work on $InAs_xP_{1-x}$ material and devices has been done because of technical problems in forming Schottky contacts with sufficiently high barrier potentials. Nevertheless, some experimental work has been done on other types of InAs and InP field-effect transistor, most notably MISFETs [4-5], and there is every reason to be optimistic that some form of heterojunction under the gate may well overcome the problem of low barrier.

Improved electron transport properties are one of the main targets in the ongoing study of binary and ternary InP, InAs and $InAs_xP_{1-x}$ materials. The Monte Carlo technique has proved valuable for studying non-equilibrated carrier transport in a range of semiconductor materials and devices [6-7]. However, carrier transport modelling of InP and InAs materials has only recently begun to receive sustained attention, now that the progress in compounds and alloys has resulted in the production of valuable materials for the electronics industry. In this communication we present Monte Carlo calculation of steady-state and transient electron transport conditions in InP, InAs and $InAs_xP_{1-x}$. We demonstrate the effect of injection energy and electric field on the transient electron transport. The differences in transport properties are analysed in terms of important material parameters.

Our current approach employs a one-dimensional ensemble Monte Carlo technique to investigate steady-state and transient electron transport in InP, InAs and $InAs_xP_{1-x}$. However, the momentum space treatment is three-dimensional and the scattering events consider all three dimensions. Specifically, our model includes the three lowest valleys of the conduction band with non-parabolicity. Details of the conduction band parameters and the Monte Carlo simulation are presented in the next section and the results of steady-state and transient transport simulations are discussed afterwards.

Model Details

Our ensemble Monte Carlo simulations of electron transport in zincblende InP, InAs and InAsxP1-x are similar to those of Arabshahi et al [8-9]. As indicated earlier, a three-valley model for the conduction band is employed.

In order to calculate the electron drift velocity for large electric fields, consideration of conduction band satellite valleys is necessary. The first-principle band structure of zincblende InAs, InP and $InAs_xP_{1-x}$ predicts a direct band gap located at the Γ point and lowest-energy conduction band satellite valleys at the *X* point and *L* point. In our Monte Carlo simulation, the Γ valley, the three equivalent *X* valleys and the four equivalent *L* valleys are represented by ellipsoidal, non-parabolic dispersion relationships of the following form [10-12]:

Maejo Int. J. Sci. Technol. **2010**, *4*(01), 159-168

$$E(k)[1+\alpha_i E(k)] = \frac{\hbar^2 k^2}{2m^*} \quad (1)$$

where m^* is effective mass at the band edge and α_i is the non-parabolicity coefficient of the *i*-th valley given by Kane model [13] as

$$\alpha_i = \frac{1}{E_g}\left[1-\frac{2m^*}{m_0}\right]\left[1-\frac{E_g\Delta}{3(E_g+\Delta)(E_g+2\Delta/3)}\right] \quad (2)$$

where E_g is the band-gap energy and Δ is the spin-orbit splitting. We assume that all donors are ionised and that the free-electron concentration is equal to the dopant concentration. For each simulation, the motion of ten thousand electron particles are examined, the temperature being set to 300 K and the doping concentration being set to 10^{17} cm^{-3}. In the case of the ellipsoidal, non-parabolic conduction valley model, the usual Herring-Vogt transformation matrices are used to map carrier momenta into spherical valleys when particles are drifted or scattered. Electrons in bulk material suffer intravalley scattering by polar optical, non-polar optical and acoustic phonon scattering, intervalley phonons, and ionised impurity scattering.

Acoustic scattering is assumed elastic and the absorption and emission rates are combined under the equipartition approximation, which is valid for lattice temperature above 77 K. Elastic ionised impurity scattering is described using the screened Coulomb potential of the Brooks-Herring model. Band edge energies, effective masses and non-parabolicity are derived from empirical pseudo-potential calculations. Important parameters used throughout the simulations are listed in Tables 1-2.

Table 1. Valley parameter selections for InAs, InP, $InAs_{0.2}P_{0.8}$ and $InAs_{0.8}P_{0.2}$ [3-5]

	InAs	InP	$InAs_{0.2}P_{0.8}$	$InAs_{0.8}P_{0.2}$
m_Γ	5667	4810	4981	5495
m_L	4280	5300	5096	4484
m_x	14.6	12.4	12.84	14.16
α_Γ	12.25	9.55	10.09	11.71
α_L	4.9	8.3	7.62	5.58
Γ-X	0.015	0.06	0.05	0.024
Γ-L	1	1	1	1

Maejo Int. J. Sci. Technol. **2010**, *4*(01), 159-168

Table 2. Material parameter selections for InAs, InP, $InAs_{0.2}P_{0.8}$ and $InAs_{0.8}P_{0.2}$ [3-5]

	InAs	InP	$InAs_{0.2}P_{0.8}$	$InAs_{0.8}P_{0.2}$
Density ρ (kgm^{-3})	5667	4810	4981	5495
Longitudinal sound velocity v_s (ms^{-1})	4280	5300	5096	4484
Low-frequency dielectric constant ε_s	14.6	12.4	12.84	14.16
High-frequency dielectric constant ε_∞	12.25	9.55	10.09	11.71
Acoustic deformation potential D(eV)	4.9	8.3	7.62	5.58
Polar optical phonon energy (eV)	0.015	0.06	0.05	0.024
Intervalley deformation potential (eVm^{-1})	1	1.1	1.05	1.065
Intervalley phonon energies (meV)	11.2	29	25.44	14.76

Results

Figure 1 shows the simulated velocity-field characteristics of zincblende InAs, InP, $InAs_{0.2}P_{0.8}$ and $InAs_{0.8}P_{0.2}$ semiconductors at 300 K, with a background doping concentration of 10^{17} cm^{-3} and with the electric field applied along one of the cubic axes. The simulations suggest that the peak drift velocity for zincblende InAs is 3.4 $\times 10^5$ ms^{-1} while that for InP, $InAs_{0.2}P_{0.8}$ and $InAs_{0.8}P_{0.2}$ are about ~ 2.3 $\times 10^5$ ms^{-1}, 2.5×10^5 ms^{-1} and 3.2×10^5 ms^{-1} respectively. At higher electric fields, intervalley optical phonon emission dominates, causing the drift velocity to saturate at around 1.5 $\times 10^5$ ms^{-1} for all materials.

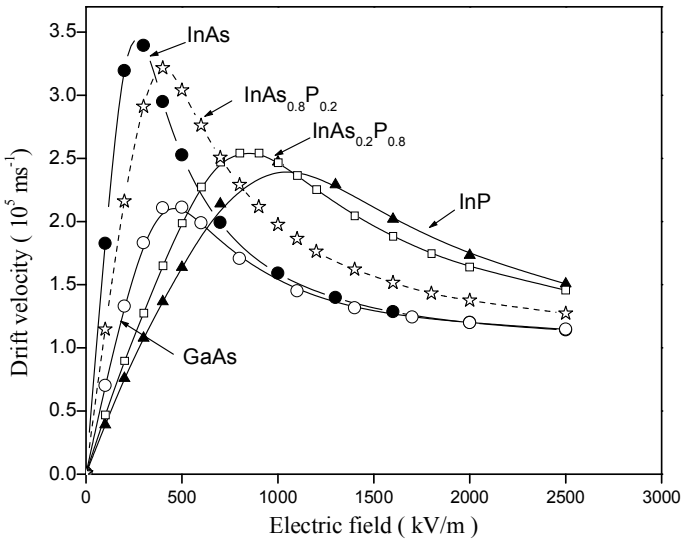

Figure 1. Calculated steady-state electron drift velocity in bulk zincblende InAs, InP, $InAs_{0.2}P_{0.8}$ and $InAs_{0.8}P_{0.2}$ at room temperature as per the non-parabolic band model

Maejo Int. J. Sci. Technol. **2010**, *4*(01), 159-168

The calculated drift velocities apparent from Figure 1 are fractionally lower than those that have been calculated by Adachi [14-16], who assumed an effective mass in the upper valleys was equal to the free electron mass. The threshold field for the onset of significant scattering into satellite conduction band valleys is a function of the intervalley separation and the density of electronic states in the satellite valleys.

The valley occupancy for the Γ, X and L valleys is illustrated in Figure 2 and shows that the inclusion of the satellite valleys in the simulation is important. Significant intervalley scattering into the satellite valleys occurs for fields above the threshold field for each material. This is important because electrons which are near a valley minimum have small kinetic energy and are therefore strongly scattered. It is apparent that intervalley transfer is substantially larger in InAs over the range of applied electric fields shown, due to the combined effect of a lower Γ effective mass, lower satellite valley separation energy, and a slightly lower phonon scattering rate within the Γ valley.

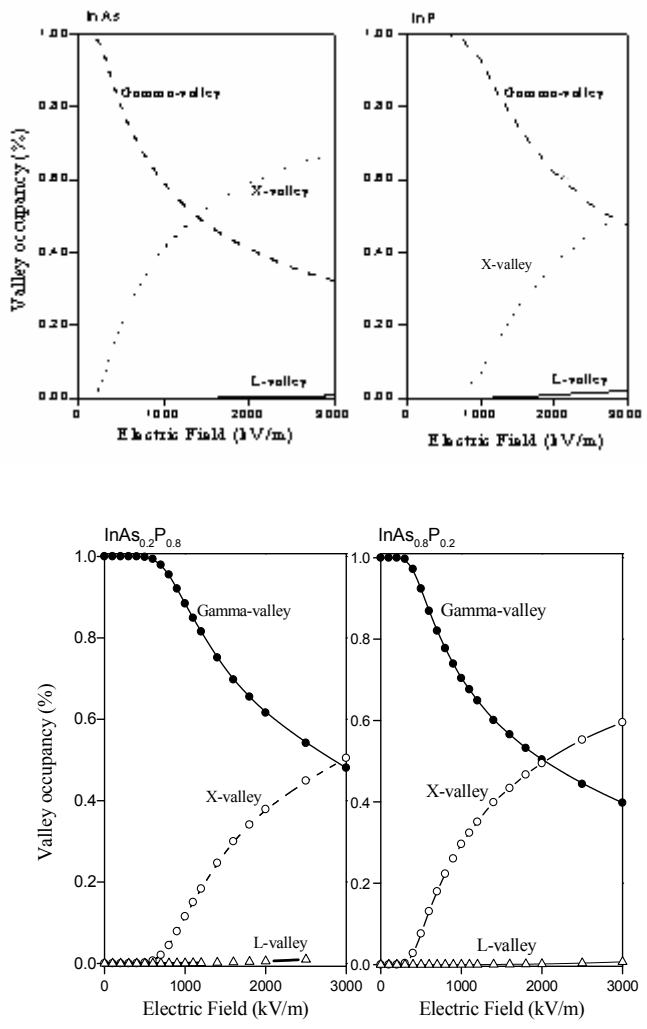

Figure 2. Fractional occupation of the central Γ and satellite valleys of zincblende InAs, InP, $InAs_{0.2}P_{0.8}$ and $InAs_{0.8}P_{0.2}$ as a function of applied electric field at room temperature as per the non-parabolic band model

Maejo Int. J. Sci. Technol. **2010**, *4*(01), 159-168

We have also examined transient electron transport in bulk InAs, InP, $InAs_{0.2}P_{0.8}$ and $InAs_{0.8}P_{0.2}$ semiconductors. The transient response of electrons in these materials are compared in Figure 3 for fields up to 1600 kVm^{-1} strength. In InAs, very little or no overshoot occurs below the threshold field of 400 kVm^{-1}. As the electric field strength is increased to a value above the threshold field, overshoot begins to occur. As the field strength is increased further, both the peak overshoot velocity increases and the time for overshoot relaxation decreases.

In InAs, the velocity overshoot initially increases more rapidly with increasing electric field due to the lower Γ valley effective mass. For example, at 1600 kVm^{-1}, the maximum overshoot velocity for InAs is about 8×10^5 ms^{-1}, whereas for InP, $InAs_{0.2}P_{0.8}$ and $InAs_{0.8}P_{0.2}$ it is about 4×10^5 ms^{-1}, 5×10^5 ms^{-1} and 7×10^5 ms^{-1} respectively. It is found also that for the same value of electric field above the threshold value, the electron drift velocity is always smaller in InP, $InAs_{0.2}P_{0.8}$ and $InAs_{0.8}P_{0.2}$ than in InAs.

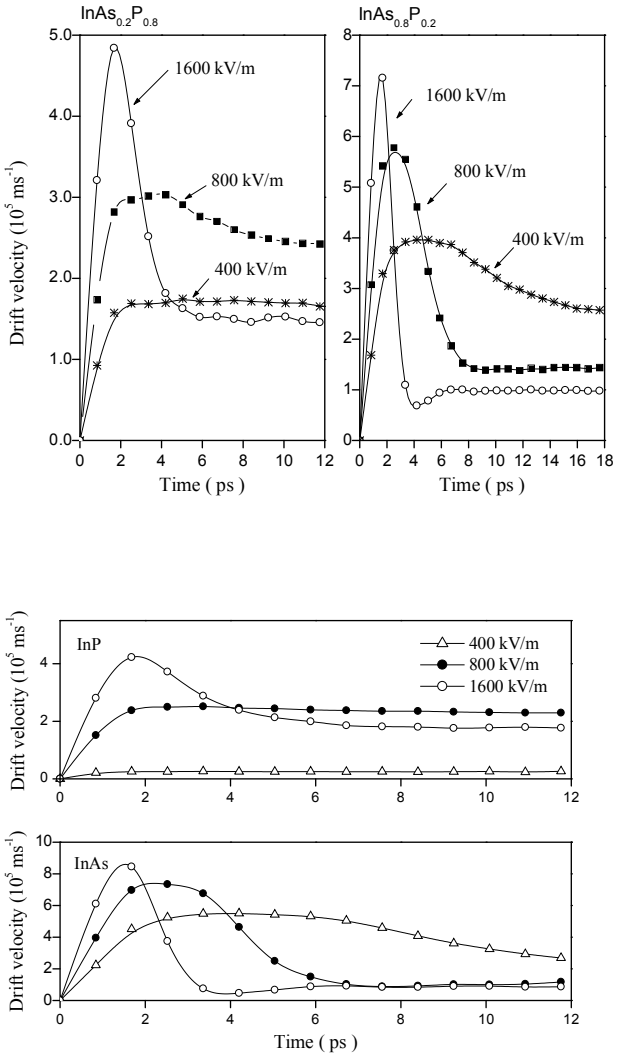

Figure 3. A comparison of the velocity overshoot effect exhibited by InAs, InP, $InAs_{0.2}P_{0.8}$ and $InAs_{0.8}P_{0.2}$ semiconductors as calculated by Monte Carlo simulation. The donor concentration is 10^{17} cm^{-3} and the temperature is 300 K.

Maejo Int. J. Sci. Technol. **2010**, *4*(01), 159-168

Figure 4 shows the average velocity of electrons in InAs, InP, $InAs_{0.2}P_{0.8}$ and $InAs_{0.8}P_{0.2}$ as a function of distance. We note that for the applied field of 400 to 1600 kVm^{-1} the average electron velocity reaches steady-state very quickly with little or no velocity overshoot. It is suggested that in $InAs_{0.2}P_{0.8}$ and $InAs_{0.8}P_{0.2}$ 400 kVm^{-1} is the critical field for the onset of velocity overshoot. As mentioned above, 400 kVm^{-1} also corresponds to the peak in the velocity-field characteristic associated with $InAs_{0.2}P_{0.8}$. Steady-state Monte Carlo simulations suggest that this is the point at which significant upper valley occupation begins to occur, as shown in Figure 2. This signifies that velocity overshoot is related to the transfer of electrons to the upper valleys. To optimise device performance, we have to minimise the transit time over a given distance.

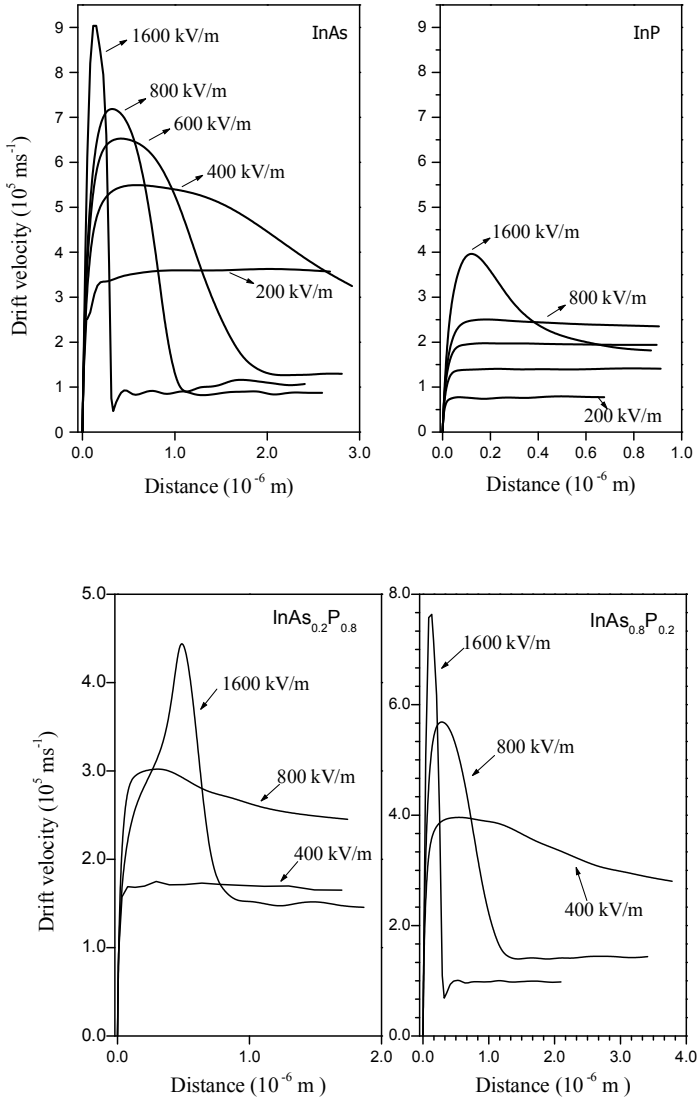

Figure 4. A comparison of the average electron velocity as a function of the displacement for various applied fields in InAs, InP, $InAs_{0.2}P_{0.8}$ and $InAs_{0.8}P_{0.2}$ semiconductors. In all cases, an initial zero field distribution, a crystal temperature of 300 K and a doping concentration of 10^{17} cm^{-3} are assumed.

Maejo Int. J. Sci. Technol. **2010**, *4*(01), 159-168

From Figure 5, it can be seen that there is a trade-off between the peak overshoot velocity and the distance taken to achieve steady state. In particular, when the applied electric field is set to 1600 kVm^{-1}, the peak overshoot velocity of $InAs_{0.8}P_{0.2}$ is 7.8×10^5 ms^{-1} while the corresponding steady-state drift velocity, 1.5×10^5 ms^{-1}, is achieved after just 0.2 μm.

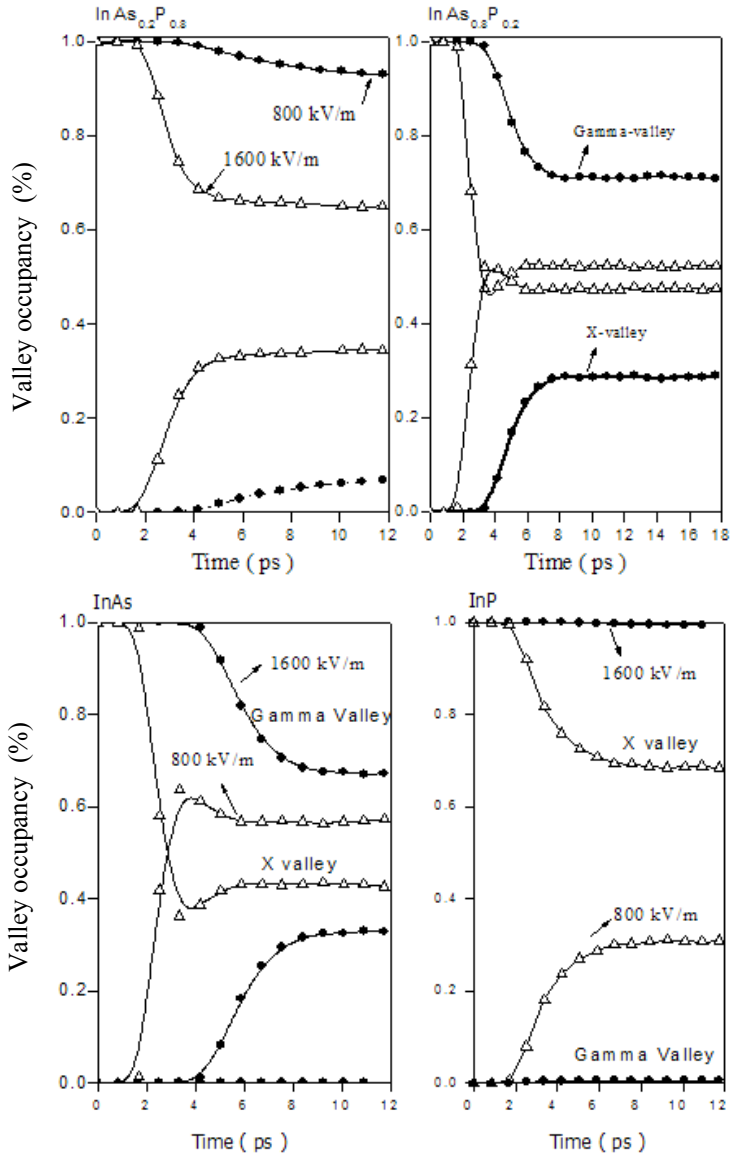

Figure 5. Comparison of the valley occupancy as a function of applied electric field in InAs, InP, $InAs_{0.2}P_{0.8}$ and $InAs_{0.8}P_{0.2}$ for Γ, *X* and *L* valleys at room temperature

However, for an applied field of 400 kVm^{-1}, just above the critical field, the peak overshoot velocity is only 4×10^5 ms^{-1} and it takes longer (about 0.8 μm) to achieve the corresponding steady-state drift velocity of 3×10^5 ms^{-1}. Similar results are noted for $InAs_{0.2}P_{0.8}$, as is seen in Figure 5. In particular, the critical field denoting the onset of velocity overshoot coincides almost exactly with the field at which the peak drift velocity in the steady-state velocity field characteristic is found, i.e. 200 kVm^{-1} for InAs and 800 kVm^{-1} for InP. The correspondence

Maejo Int. J. Sci. Technol. **2010**, *4*(01), 159-168

between the critical field at which the onset of velocity overshoot effect occurs and the peak in the steady-state velocity field characteristic appears to be valid for the case of other III-V semiconductors as well.

Conclusions

Electron transport at 300 K in bulk zincblende InAs, InP, $InAs_{0.2}P_{0.8}$ and $InAs_{0.8}P_{0.2}$ has been simulated using an ensemble Monte Carlo simulation. Using valley models to describe the electronic bandstructure, calculated velocity-field characteristics are in fair agreement with other calculations. Saturation drift velocities ($\sim 1.5\times10^5$ ms^{-1}) match recent measurements on low-doped bulk samples. The velocity-field characteristics of the materials show similar trends, reflecting the fact that all the semiconductors have satellite-valley effective densities of states several times greater than the central Γ valley. However, the peak velocity in $InAs_{0.2}P_{0.8}$ occurs at a field ~ 700 kVm^{-1}, twice larger than that for $InAs_{0.8}P_{0.2}$. This is a consequence of the large Γ valley effective mass in $InAs_{0.2}P_{0.8}$ structure. This reduced valley effective mass in $InAs_{0.8}P_{0.2}$ permits substantial population of the upper valleys and velocity saturation at far lower electron temperature than that for InP.

Acknowledgement

We would like to thank M. G. Paezi for her useful comments.

References

1. K. Brennan, K. Hess, J. Y. Tang and G. J. Iafrate, "High field electron transport properties", *IEEE Trans. Electron Devices*, **1983**, *30*, 1750-1755.
2. N. Newman, T. Kendelewicz, L. Bowman and W. E. Spicer, "Electron transport properties in nitrides semiconductor devices", *Appl. Phys. Lett.,* **1985**, *46*, 1176-1181.
3. N. Newman, V. Schilfgaarde, T. Kendelewicz and W. E. Spicer, "Monte Carlo studies in two dimensional GaN/AlGaN devices", *Mater. Res. Soc. Symp. Proc.,* **1986**, *54*, 443-449.
4. D. C. Cameron, L. D. Irving and C. R. Whitehouse, "Hot carrier relaxation in InP and GaAs", *Thin Solid Films.,* **1983**, *103*, 61-66.
5. D. C. Cameron, L. D. Irving and C. R. Whitehouse, "Ensemble Monte Carlo simulation in InP and InN", *Electron. Lett.*, **1982**, *18*, 534-538.
6. C. Moglestue, "Monte Carlo Simulation of Semiconductor Devices", Chapman and Hall, New York, **1993**.
7. C. Jacoboni and P. Lugli, "The Monte Carlo Method for Semiconductor and Device Simulation", Springer-Verlag, New York, **1989**.

Maejo Int. J. Sci. Technol. **2010**, *4*(01), 159-168

8. H. Arabshahi, M. R. Benam and B. Salahi, "Comparison of high field and steady-state transient electron transport properties in GaN, InN and AlN", *Modern Phys. Lett. B.*, **2007**, *21*, 1715-1721.
9. H. Arabshahi, "Comparison of high field steady state transport properties in zincblende and wurtzite GaN", *Modern Phys. Lett. B.*, **2007**, *21*, 199-206.
10. B. E. Foutz, L. F. Eastman, U. V. Bhapkar and M. Shur, "Full band Monte Carlo simulation of zincblende GaN MESFET's including realistic impact ionization rates", *Appl. Phys. Lett.,* **1997**, *70*, 2849-2854.
11. U. V. Bhapkar and M. S. Shur, "Ensemble Monte Carlo study of electron transport in wurtzite InN", *J. Appl. Phys.,* **1997**, *82*, 1649-1654.
12. J. D. Albrecht, R. P. Wang, P. P. Ruden and K. F. Brennan, "Monte Carlo simulation of GaN in zincblende and wurtzite structures", *J. Appl. Phys.,* **1998**, *83*, 2185-2190.
13. E. O. Kane, "Band structure calculation in group III and IV materials", *J. Phys. Chem. Solids,* **1957**, *1*, 249-253.
14. S. Adachi, "GaAs and Related Materials, Bulk semiconducting and Superlattice Properties", World Scientific, Singapore, **1994**.
15. S. Adachi, "Physical Properties of III-V Semiconductor Compounds, InP, InAs, GaAs, GaP,AlAs and AlGaAs", Wiley, New York, **1992**.
16. S. Adachi, "Properties of AlGaAs", INSPEC, Stevenage (UK), **1993**.